Journal of Materials Science: Materials in Electronics (2019) 30:20320–20329
https://doi.org/10.1007/s10854-019-02394-7

REVIEW

Potential challenges and approaches to develop the large area efficient monolithic perovskite solar cells (mPSCs)

Arti Mishra[1] · **Zubair Ahmad**[1]

Received: 8 August 2019 / Accepted: 16 October 2019 / Published online: 12 November 2019

Abstract

The next generation technologies based on perovskite solar cells (PSCs) are targeted to develop a true low cost, low tech, widely deployable, easily manufactured and reliable photovoltaics. After the extremely fast evolution in the last few years on the laboratory-scale, PSCs power conversion efficiency (PCE) reached over 24%. However, the widespread use of PSCs requires addressing the stability and industrial scale production issues. Carbon based monolithic perovskite solar cells (mPSCs) are one of the most promising candidates for the commercialization of the PSCs. mPSCs possess a unique architectural design and pave an easy way to produce large area and cost-effective fabrication of the PSCs. In this article, recent progress in the field of mPSCs, challenges and strategies for their improvement are briefly reviewed. Also, we focus on the predominant implementations of recent techniques in the fabrication of the mPSCs to improve their performance. This review is intended to serve as a future direction guide for the scientists who are looking forward to developing more reliable, cost-effective and large area PSCs.

1 Background

The first monolithic photovoltaic (PV) device was reported by Kay and Grätzel [1] in 1996. They fabricated a monolithic device consist of a transparent SnO_2 layer on a glass substrate, a mesoporous TiO_2 layer, an insulating ZrO_2 layer and a counter carbon electrode (as shown in Fig. 1a). Carbon electrode was made up with carbon paste consists of graphite powder, carbon black and using TiO_2 as a binder. The pores of mesoporous layers were filled with a redox electrolyte to facilitate the transportation of the charge carriers between the SnO_2 and carbon respectively. The photo conversion efficiency (PCE) of these individual monolithic cells was 6.67%. Further, series connection of the mPSCs on the SnO_2 substrate were accomplished to prepare a solar cell module and a PCE value of 5.29% was recorded over the area of 21.67 cm^2 [1]. This work successfully demonstrated the working principle of the monolithic PV devices and provide enough background to make a monolithic solar cell module for scale up fabrication. However, this module had drawbacks associated with liquid electrolyte. Particularly, the carbon layer was swelled after electrolyte absorption. Hence this liquid monolithic solar cell was needed to modify into solid state monolithic cells.

In 2013 Ku et al. [2] reported the first solid state mPSCs device using the carbon black/spheroidal graphite and obtained a PCE value of 6.64%. This device exhibited a stable performance over 800 h at room temperature. This work initiated the research towards the cost-effective carbon-based solid state mPSCs. Later, this group did a series of researches to improve carbon electrode-based hole transport layer (HTL) free mPSCs. To improve the PCE, in the following work, an ordered mesoporous carbon (OMC) was mixed with flaky graphite to prepare a carbon paste which was employed to fabricate the mPSCs. OMC is extensively used as an electrode material for electrochemical applications, due to its good surface morphology, consistent and tunable pore sizes and physicochemical properties. However, due to its low conductivity, the carbon paste was not suitable for mPSCs electrodes and hence it was mixed with graphite [3]. For further improvement, they used TiO_2 nano-sheets and employ two step sequential deposition of perovskite liquid. Initially, PbI_2 were coated by spin coating, then cells were dipped into the MAI solution for 10 min. This process enhances the electrical linking between layers hence 10.64% PCE was attained [4]. This was further improved to 11.6% PCE by optimizing the thickness of the carbon

✉ Zubair Ahmad
zubairtarar@qu.edu.qa

[1] Center for Advanced Materials (CAM), Qatar University, P. O. Box 2713, Doha, Qatar

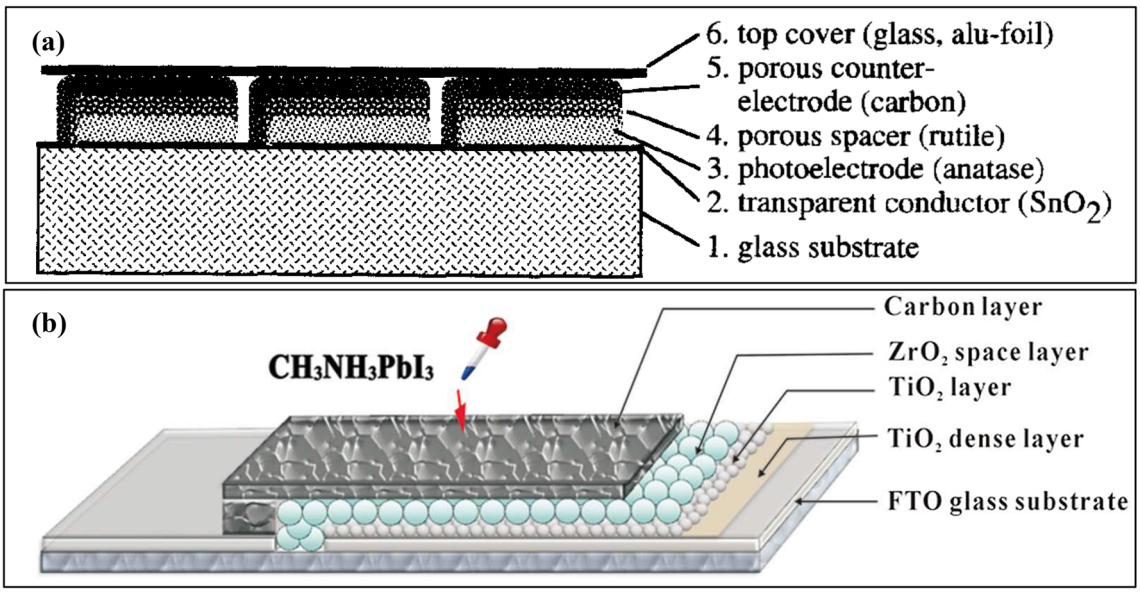

Fig. 1 **a** Cross sectional representation of the used monolithic dye sensitized solar cells using liquid electrolyte. (Reprinted with permission from [1], copyright (1996) Elsevier). **b** A schematic representation of solid state mPSCs device using perovskite as photo sensitizer (Reprinted with permission from [2], copyright (2013) Springer Nature)

counter electrode and the size of flaky graphite particle used in carbon slurry [5].

In 2014, Mei et al. [6] published a benchmark work which pushes mPSCs towards stability and scalability, they infiltrated mesoporous layers with $(5\text{-AVA})_x(MA)_{1-x}PbI_3$ to substitute $MAPbI_3$ [6]. The perovskite solution was formed in two steps, first by mixing 5-ammoniumvaleric acid iodide (5-AVAI) with methylammonium iodide (MAI), this solution was further mixed with lead iodide (PbI_2) in γ-butyrolactone. Organized 5-AVA^+ cations swapped MA cations in the cuboctahedral location of conventional perovskite and creating novel mixed-cation perovskite with orthorhombic phase. The 5-AVA molecules formed extended hydrogen-bonded chains among COOH and NH_3^+ groups and I^- ions from the PbI_6 octahedra, which behaves as a stimulating agent to produce mixed-cation perovskite $(5\text{-AVA})_x(MA)_{1-x}PbI_3$. Crystals made with this hybrid perovskite possessed minor imperfection and presented enhanced pore filling across the TiO_2, ZrO_2, and carbon scaffolds, hence created better crystallinity network between the layers. This mPSCs was revealed with a certified PCE of 12.84%, with a very less value of hysteresis and a high value of J_{sc} (22.8 mA/cm^2). This device was tested under 1 sun without any encapsulation and the device stability was more than one 1000 h. The 5-AVA cations govern growth of perovskite crystals in the deep porous cavities of TiO_2 layer. The device made with conventional $MAPbI_2$ perovskite revealed unoccupied nanopore in the mesoporous layers due to the faster precipitate formation of $MAPbI_2$ [6]. After these initial works many reports have been described (summarized in Table 1) to improve mPSCs device by mesoporous layers and perovskite liquid improvement.

Here it is also important to highlight that typically PSCs are consist of anode/ETL/perovskite/HTL/cathode (n–i–p) structure. The perovskite layer absorbs the incident photons and generate electrons and holes, which are separated by the electron transport layer (ETL) and the hole transport layer (HTL) and further move towards the anode and cathode of the cell creating the flow of electric current. The metal electrodes are deposited under high vacuum by physical vapor deposition (PVD) while the other layers are usually spin coated for PSCs fabrication. The PVD and spin coating processes are only appropriate for small scale fabrication. Due to all above stated reason, in spite of attaining high efficiency, PSCs are very far from commercial manufacturing [20]. Henceforward fabrication protocols for all the layers which is easily acceptable for large area PSCs manufacturing are highly desired.

2 Challenges to develop the large area mPSCs

The 1st challenge is to develop or optimize the cost-effective technique for the infiltration of perovskite precursor ink with very high reproducibility. It is highly desirable to optimize the infiltration procedure for the mPSCs to prepare the devices with high yield. The inkjet infiltration technique demonstrates noteworthy performance and reproducibility. It opens new paths for batch printing [16], nevertheless the

Table 1 Summary of the work done on the HTL-free (carbon-based) mPSCs

S.No	$mTiO_2$ thickness (μm)	$mZnO_2$ thickness (μm)	mCarbon thickness (μm)	Type of carbon electrode	Perovskite composition	Infiltration (step)	PCE (%)	Year
1	10	10	60	Graphite/carbon black paste (GCBP)	NA	NA	6.67	1996 [1]
2	1	1	10	Spheroidal graphite	$CH_3NH_3PbI_3$	1	6.64	2013 [2]
3	1	1	10	flaky graphite	$CH_3NH_3PbI_3$	1	4.08	2013 [2]
4	1	2	NA	OG15	$CH_3NH_3PbI_3$	1	7.02	2014 [3]
5	1	2	NA	OG16	$CH_3NH_3PbI_3$	1	6.3	2014 [3]
6	0.6	1	10	Carbon slurry	PbI_2 →MAI	2	10.64	2014 [4]
7	1	2	10	GCBP	$(5\text{-AVA})_x(MA)_{1-x}PbI_3$	1	12.84	2014 [6]
8	0.4	0.5	5	GCBP	PbI_2 →MAI	2	9.79	2015 [5]
9	0.4	0.5	7	GCBP	PbI_2 →MAI	2	10.02	2015 [5]
10	0.4	0.5	9	GCBP	PbI_2 →MAI	2	11.63	2015 [5]
11	0.4	0.5	12	GCBP	PbI_2 →MAI	2	10.56	2015 [5]
12	0.4	0.5	15	GCBP	PbI_2 →MAI	2	10.53	2015 [5]
13	2	1	9	GCBP	PbI_2 →MAI	2	12.7	2015 [7]
14	1	2	10	GCBP	$(5\text{-AVA})_x(MA)_{1-x}PbI_3$	1	13.41	2015 [8]
15	0.5	0	10	GCBP	$CH_3NH_3PbI_3$	1	1.56	2015 [9]
16	0.5	0.3	10	GCBP	$CH_3NH_3PbI_3$	1	5.92	2015 [9]
17	0.5	0.5	10	GCBP	$CH_3NH_3PbI_3$	1	9.02	2015 [9]
18	0.5	1	10	GCBP	$CH_3NH_3PbI_3$	1	10.30	2015 [9]
19	0.5	1.4	10	GCBP	$CH_3NH_3PbI_3$	1	9.29	2015 [9]
20	1	2	10	GCBP	$(5\text{-AVA})_x(MA)_{1-x}PbI_3$	1	12.9	2015 [10]
21	0.4	1.5	10	GCBP	$CH_3NH_3PbI_{(3-x)}(BF_4)_x$	1	13.24	2016 [11]
22	1	2	10	GCBP	$CH_3NH_3PbI_3$	1	13.89	2016 [12]
23	0.5	2	10	carbon paste	$CH_3NH_3PbI_3$ +LiCl	1	14.5	2016 [13]
24	0.3	0.6	15	GCBP	$CH_3NH_3PbI_3$	1	7.2	2016 [14]
25	1	2	10	Carbon paste	$MAPbI_3$ *x*GuCl	1	14.35	2017 [15]
26	0.3-0.6	1-2	10-12	Commercial Carbon paste (CCP) (Solaronix)	$(5\text{-AVA})_x(MA)_{1-x}PbI_3$	Inkjet	8.15	2017 [16]
27	0.3-0.6	1-2	10-12	CCP	$(5\text{-AVA})_x(MA)_{1-x}PbI_3$	Inkjet	6.56	2017 [17]
28	0.3-0.6	1-2	10-12	CCP	$(5\text{-AVA})_x(MA)_{1-x}PbI_3$	Inkjet	14.3	2017 [18]
29	1	2	10	CCP	$(5\text{-AVA})_x(MA)_{1-x}PbI_3$	1	14.02	2017 [19]

use of this technique is mainly limited by quick conversion of perovskite liquid precursors to perovskite crystals, hence the nozzles of the printer cartridges experience blockage very rapidly and stop working for specific materials deposition. Even the introduction of additives in the perovskite precursor solution could not completely solve the problem of the nozzle blockage in the inkjet infiltration procedure. Furthermore, the maintenance and the capital cost of the inkjet printer for the perovskite precursor is also very high. To avoid the nozzle blockage issue either the new inkjet printing compatible precursor inks must be prepared or the new deposition methods should be explored.

The 2nd challenge under debate is to slow down the perovskite crystal growth and to the enhance the flow rate of perovskite ink during the infiltration process. The crystal size and crystallinity of perovskite can be well controlled by additives. The addition of the additives can significantly slow down the perovskite crystal growth before and after the admission of the precursor ink into the mesoporous layers. The 5-AVA cations govern development of perovskite crystals in the deep porous cavities of TiO_2 layer and encourage superior crystal development in the regular direction. The proper filling of perovskite liquid in the mesoporous layers ($mZrO_2$ and $mTiO_2$) strongly depends upon the droplet size, drop release timing and drop location (gap between the drops) [21]. The other comprehensive studies on this issue indicate that the viscosity of liquid, pore size and surface area of mesoporous layers are also important the factors which need to be carefully optimized [22, 23]. There is need to perform the engineering of the mesoporous (TiO_2

and ZrO_2) layers to optimize the pore to enhance the flow rate of the perovskite precursors. Here it is important to note that the supreme pore filling within the pores governs by the many parameters. The proper size of TiO_2 nanoparticle guide perovskite liquid during infiltration and help to provide good contact between perovskite liquid and TiO_2 particles [8]. By improving the wettability of the infiltration fluid, the pore filling capability and the flow rate of liquid can be enhanced [24]. The temperature of the perovskite precursor solution and monolithic substrate at the time of perovskite infiltration must be well controlled.

The 3rd main challenge is the Stability of mPSCs. There is a research gap remained to perform the systematic studies on the stability, degradation and charge transport properties in mPSCs. Even though the stability has been achieved for more than 10,000 h [25] in a specific environment, but the further work is highly necessary to make the mPSCs stable in the harsh environment. It has been shown that guanidinium (Gu) greatly improve the stability of perovskite films when mixed with $MAPbI_3$ precursor [26]. The introduction inorganic cesium (Cs) also improves PSCs and produce high efficiency reproducible device [27]. The addition of four cations (methylammonium (MA), formamidnium (FA), Cs, and Gu) can increase efficiency and stability even further [28]. The above stated triple cation and quadruple-cation perovskites which has been produced efficient and stable device in mesoporous planner architecture with gold as top electrode. However, these perovskite precursors have not been introduced in mPSCs due to the infiltration limits in mPSCs.

If the above-mentioned challenges are properly addressed, then the mPSCs can be easily penetrated the commercial market. Table 2 summarize the recent work on the on large area printable mPSCs.

3 Approaches used to improve the mPSCs

3.1 Structural design optimization

Size of the TiO_2 particles is a crucial component for a virtuous mPSCs. The size of the TiO_2 nanoparticle guide perovskite liquid during infiltration and help to provide good contact between perovskite liquid and TiO_2 particles. Yang et al. [8] performed characterization of mPSCs based on the size of TiO_2 nanoparticle. They employed four different sizes (10, 15, 20, 25 nm) of TiO_2 nanoparticles to fabricate TiO_2 mesoporous layer and obtained the highest efficiency (13.4% PCE) using the 25 nm TiO_2 nanoparticles [8]. $mTiO_2$ using the inkjet printing has also applied to deposit the highly reproducible and symmetrical mesoporous layers [28]. Liu et al. [9] investigated the different thickness (0.3, 0.5, 1 and 1.4 μm) of the ZrO_2 layers. Maximum efficiency has been found at 1 μm thick ZrO_2 layer. In this work temperature of the perovskite precursor solution and temperature of the monolithic cell at the time of perovskite infiltration have been also studied. 12.34% PCE was obtained when the temperatures of the both monolithic cell and precursor solution was kept at 70 °C, however, maximum short circuit current was obtained using 1.4 μm thick ZrO_2 layer [9]. Champion device (with 13.14% PCE) were fabricated by using the controlled parameters such as filling volume of perovskite, ZrO_2 thickness and process temperature. Al_2O_3 and SiO_2 [30] have been also investigate as space layer, but their performance has been found inferior as compared to $mZrO_2$.

Effect of different polar solvents such as DMF, DMSO, γ-butyrolactone (GBL), and 1-methyl-2-pyrrolidinone (NMP), on the wettability of the perovskite precursor solutions, have been investigated by Chen et al. [12]. The stability of intermediate phase and mPSCs performance has been thoroughly examined and found that DMF and DMSO based solutions possess the better characteristics than GBL and NMP. For further characterization DMF and DMSO was mixed in proper proportion and champion device has been produced with 13.89% PCE. In this work it has been proven that wettability of perovskite precursor solution on mesoporous layers of mPSCs is strongly influenced by the polarity and the viscosity of solvents [12].

Liu et al. [7] enhanced TiO_2 and perovskite interface by introducing a self-assembled organic silane monolayer by solvent treatment. The mPSCs has been immersed in aminopropyltrimethoxysilane ($C_6H_{17}NO_3Si$ /0.05 mM) in 2-propanol solvent for few hours to build silane monolayer, washed in 2-propanol and dried under nitrogen. This process form contacts between titanium and silicon and by

Table 2 Summary of the recent work done on large area printable mPSCs

S. No	$mTiO_2$ thickness (μm)	$mZnO_2$ thickness (μm)	mCarbon thickness (μm)	Perovskite	Active area (cm^2)	Stability (h)	PCE (%)	Year
1	0.5	1.4	10–12	$(5\text{-AVA})_x(MA)_{1-x}PbI_3$	31	2000	10.46	2016 [21]
2	0.5	1.4	10–12	$(5\text{-AVA})_x(MA)_{1-x}PbI_3$	70	2000	10.74	2016 [21]
3	1	2	10	$(5\text{-AVA})_x(MA)_{1-x}PbI_3$	49	1000	10.4	2017 [19]
4	1	2	10	$(AVA)_x(MA)_{1-x}PbI_3$	47.6	12,000	11.2	2017 [25]
5	0.5	1.3	10–12	$(5\text{-AVA})_x(MA)_{1-x}PbI_3$	70	2500	11.06	2018 [29]

forming Ti–Si bonds and attaching $NH_2(CH_2)_3$ across the perovskite. This surface modification of mesoporous TiO_2 not only enhance band alignment between the mesoporous layers but also passivate the recombination of charges at the center of layers, hence able to produce 12.7% PCE. For improving the mPSCs performance, the zinc tin oxide (ZTO) has been introduced as electron transport layers (ETL) by Zhao et al. [31]. The ZTO films have been prepared by mixing Di-n-butyltin bis(2,4-pentanedionate) ($C_{18}H_{32}O_4Sn$) and zinc acetate dihydrate [$Zn(CH_3COO)_2{\cdot}2H_2O$] in different weight percentage in methanol solvent and printed using spray pyrolysis. The use of ETL suppresses energy loss and supplements the V_{oc} due to the suitable matching of cascade level between perovskite and the ZTO ETL as shown in Fig. 2. The champion device produces a high V_{oc} of 1.02 V and PCE of 15.86% and long-term stability using$(5\text{-AVA})_x(MA)_{1-x}PbI_3$ perovskite precursor. These findings provide a simple pathway to design the interface between ETL and perovskite, and to tailor the band alignment to suppress interfacial trap-assisted recombination of mPSCs for enhancing V_{oc} and charge extraction simultaneously [31].

3.2 Use of additives or dopants in perovskite precursor solutions

Based on the coordination, interaction of different components and the colloidal characteristic of precursor solution, the crystal size and crystallinity of perovskite can be well controlled using additives. Many additives have been proposed to mix with perovskite precursor solutions to improve the PCE of the mPSCs (as shown in Table 3). [6,6]-Phenyl-C_{61}-butyric acid methyl ester (PCBM) has been supplemented with two types of perovskite [$MAPbI_3$ and $MAPbI_{2.95}(BF_4)_{0.05}$] precursor solutions by Guan et al. [32]. By adding 0.25 mg / ml PCBM in $MAPbI_3$ and $MAPbI_{2.95}(BF_4)_{0.05}$ precursors, the PCEs of mPSCs have been enhanced from 8.58% to 12.36% and 12.77% to 14.26%, respectively. The PCBM additive improve perovskite morphology, stimulate charge separation and diminish charge recombination in the mPSCs device [32]. In another work Zou et al. [33] varied carbon quantum dots (CQDs) in the perovskite precursor solution before infiltration. It has been found that the little addition of CQDs to the perovskite solution can enhance the photocurrent density of mPSCs [33].

In another report, a bifunctional 4-(amin omethyl) benzoic acid hydroiodide (AB) was added to $MAPbI_3$ precursor and the results were compared with the monofunctional cation benzylamine hydroiodide (BA) and nonconjugated bifunctional organic molecule 5-ammonium valeric acid (5-AVA). Devices based on AB+$MAPbI_3$ show a good stability with a maximum PCE of 15.6%. The SEM analysis of the films made with the above mentioned three precursor solutions is shown in the Fig. 3. The SEM images of the AB+$MAPbI_3$ (Fig. 3c, d) and AVA + $MAPbI_3$ (Fig. 3e, f) films showed a superior pore-filling due to the COOH groups anchored to the AB and AVA. The bifunctional conjugated cation not only contribute during the growth of perovskite crystals in the mesoporous network but also facilitates the charge transport. This investigation helped to explore the new approaches to rationalize the design of the organic cations for perovskite materials [34]. An alternative approach was also applied by using a molten-salt-based $MAPbI_3$ precursor solution, in the nano porous graphite based monolithic cells and stabilized photovoltage as high as 1 V (the highest V_{oc} reported for HTL-free $MAPbI_3$ based devices) has been achieved [35]. 5AVAI has also been used as an additive in $MAPbI_3$ perovskite liquid and the performance of the cells has been significantly improved.

Chen et al. [11] developed a mixed-anion perovskite $CH_3NH_3PbI_{(3-x)}(BF_4)_x$. They reported that the replacement of I^- by BF_4^- expressively enhance light harvesting ability,

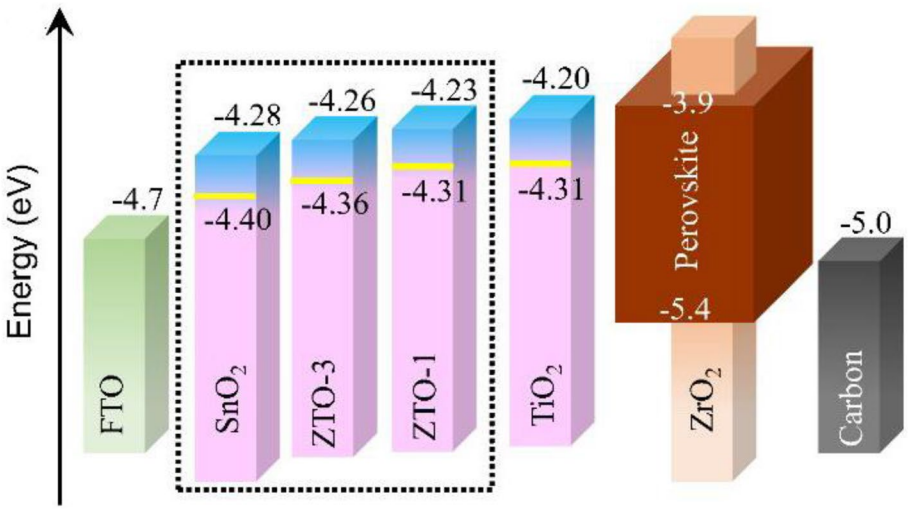

Fig. 2 Possible band alignment of perovskite solar cell based on different Electron Transport Layer according to their fermi levels, conduction bands and bandgaps (Reprinted with permission from [31], copyright (2019) American Chemical Society)

Table 3 Recent reports on mPSCs using additives in perovskite precursors

S.No.	$mTiO_2$	$mZrO_2$	m-C	Comment	PCE(%)	Year
1	600 nm	2 µm	12 µm	$MAPbI_3$ (reference sample without additive)	8.58	2018 [32]
2	600 nm	2 µm	12 µm	$MAPbI_3$ wih PCBM (0.25 mg /ml)	12.36	2018 [32]
3	600 nm	2 µm	12 µm	$MAPbI_{2.95}(BF_4)_{0.05}$	12.77	2018 [32]
4	600 nm	2 µm	12 µm	$MAPbI_{2.95}(BF_4)_{0.05}$ with PCBM (0.25 mg /ml)	14.26	2018 [32]
5	–	–	–	$MAPbI_3$ with 5% carbon quantum dots (CQDs)	7	2018 [33]
6	500 nm	2 µm	15 µm	$MAPbI_3$	6.47	2018 [34]
7	500 nm	2 µm	15 µm	$MAPbI_3$ with benzylamine hydroiodide (BA)	12	2018 [34]
8	500 nm	2 µm	15 µm	$MAPbI_3$ with 5-aminovaleric acid hydroiodide (AVA)	14.1	2018 [34]
9	500 nm	2 µm	15 µm	$MAPbI_3$ with 4-(aminomethyl) benzoic acid hydroiodide (AB)	15.6	2018 [34]
10	700 nm	1.6 µm	9 µm	Molten-salt-based $MAPbI_3$ precursor solution	12.6	2018 [35]
11	500 nm	3 µm	10 µm	Room-temperature liquid metals added with carbon paste	13.51	2018 [40]
12	600 nm-NR18	–	10 µm	$Cs_{0.1}FA_{0.9}PbI_3$	9.35	2019 [39]
13	600 nm-NR30	–	10 µm	$Cs_{0.1}FA_{0.9}PbI_3$	13.92	2019 [39]
14	600 nm-NR30	1.2 µm	10 µm	$Cs_{0.1}FA_{0.9}PbI_3$	8.02	2019 [39]
15	600 nm-NR30	2 µm	10 µm	$Cs_{0.1}FA_{0.9}PbI_3$	14.38	2019 [39]
16	600 nm-NR30	3 µm	10 µm	$Cs_{0.1}FA_{0.9}PbI_3$	12.74	2019 [39]
17	500 nm	2 µm	10 µm	ZTO-3 (20 nm) and ZTO-1 (50 nm) printed between FTO and $mTiO_2$	15.86	2019 [31]

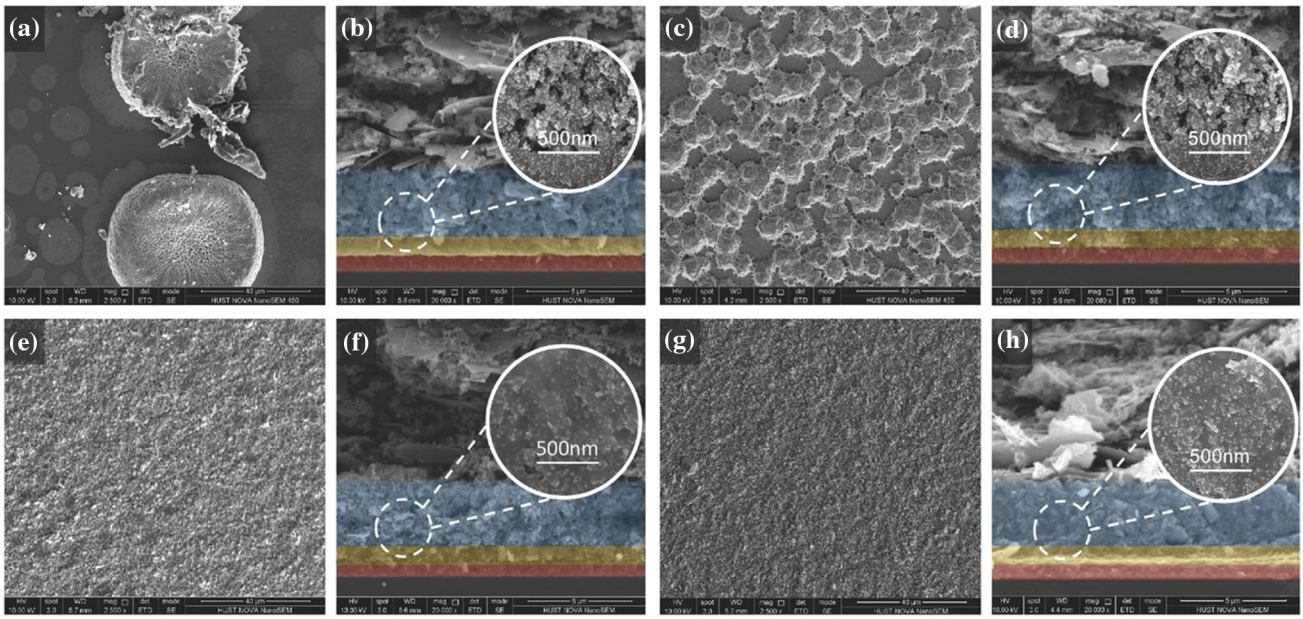

Fig. 3 The top view scanning electron microscopy (SEM) images for **a** $MAPbI_3$, **c** AB+ $MAPbI_3$, **e** AVA+$MAPbI_3$, and **g** AB+$MAPbI_3$ on 500 nm TiO_2/2 µm ZrO_2 and their cross-sectional SEM images of the cells filled with **b** $MAPbI_3$, **d** AB+ $MAPbI_3$, **f** AVA+$MAPbI_3$, and **h** AB-$MAPbI_3$ on 500 nm TiO_2/2 µm ZrO_2 (Reprinted with permission from [34], Copyright (2018) Wiley Online Library)

carrier concentration and conductivity of the device which results boost in PEC (0.54% with $CH_3NH_3PbI_3$) to [13.24% with $CH_3NH_3PbI_{(3-x)}(BF_4)_x$] [11]. For further improving perovskite solution pore filling, Sheng et al. [36] mixed Lithium chloride (LiCl) with perovskite solution in 10, 20, and 30 wt%. The LiCl-mixed perovskite revealed higher electronic properties due to quicker electron transference. With 30 wt% of LiCl in perovskite precursor a PCE value of 14.5% was attained [13]. Furthermore, guanidinium chloride (GuCl) additive has been introduced by Hou et al. [15]. The Gu cation-built a cross-link connection between the adjoining jots of perovskite shown in Fig. 4 results in the crack free morphology of perovskite crystal. It has been experienced in this work that iodide ions possess inferior electronegativity

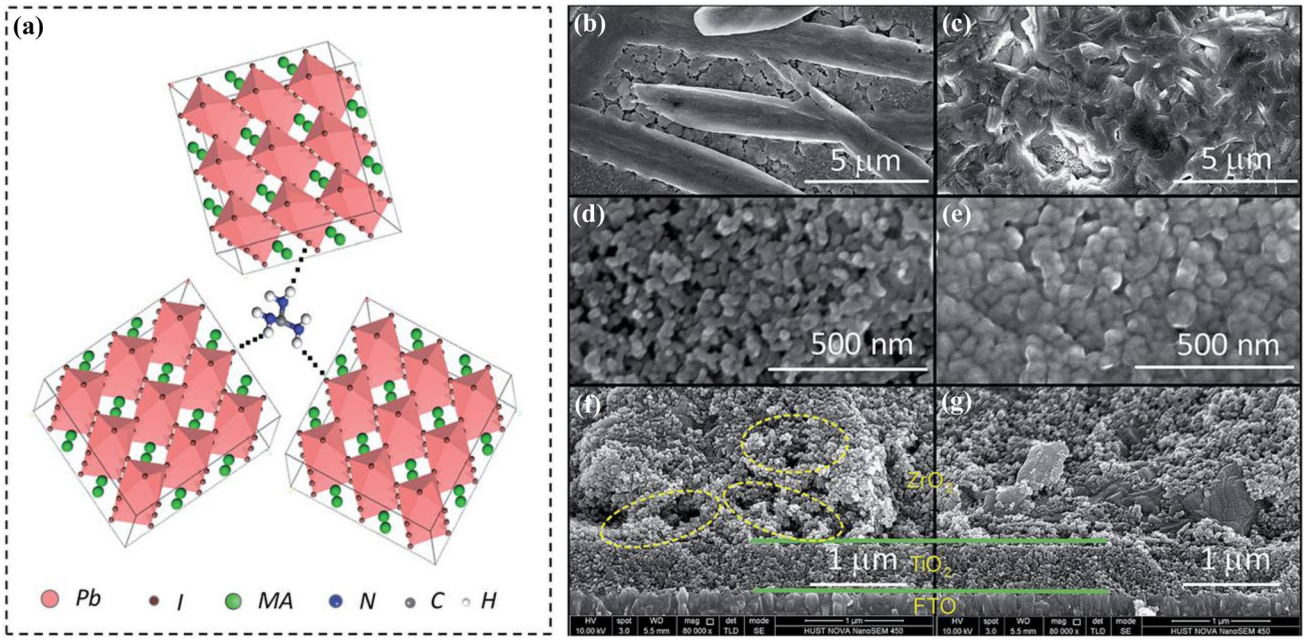

Fig. 4 **a** Representation of crosslinked perovskite grains under the influence of GuCl. **b**, **c** SEM images of $MAPbI_3$ and $MAPbI_3$ xGuCl films on FTO substrates. **d**, **e** SEM images of $MAPbI_3$ and $MAPbI_3$ xGuCl infiltrated $mTiO_2$ layer; (f and g) cross sectional SEM images of them TiO_2 and $mZrO_2$ with $MAPbI_3$ and $MAPbI_3$ xGuCl (x = 0.25) perovskite (Reprinted with permission from [15], copyright (2017) Royal Society of Chemistry)

than the chloride ions. This results up-field swing in the resonance signals and hence the V_{OC} of the mPSCs were improved from 0.88 V to 1.02 V with 14.27% PCE [15]. An inorganic caesium (Cs) cation has also been incorporated into the perovskite and 15% PCE was obtained with superior thermal and operational stabilities [37].

Zong et al. [38] added ammonium chloride (NH_4Cl) in perovskite precursor solution to demonstrate stability improvement of mPSCs by using simple solution-process [38]. Hou et al. [39] applied formamidinium lead triiodide ($Cs_{0.1}FA_{0.9}PbI_3$) as the light synthesizer. In this work high-quality α-$Cs_{0.1}FA_{0.9}PbI_3$ phase inside the mesoporous scaffold has been built using a mixed solvent of DMF and DMSO, and further adding CsI in the precursor solution. The vapor assisted crystallization approach has been used to produc 15% PCE with a spectral response up to 840 nm. The phase transition and crystal growth of $Cs_{0.1}FAPbI_3$ were carefully monitored in the mesoporous scaffold [39].

3.3 Use of different perovskite precursor infiltration techniques

For perovskite infiltration usually, one-step drop casting or two-step dip coating deposition methods has been used. However, these manual perovskite infiltration methods which has been feasible for small area devices are not applicable for large-scale commercial fabrication of mPSCs. Hashmi et al. [16–18] performed series of work to address issue of manual perovskite infiltration across mPSCs. They introduced fully printable mPSCs in ambient conditions with inkjet printing of perovskite as illustrated in Fig. 5. With this procedure highly reproducible devices have been fabricated having 8.15% PCE. These devices withstand for 1046 h for extended light soaking stability test at 35 °C under 1 sun without any degradation [16]. Same mPSCs devices were also tested for intense ultra-violet light soaking for 1002 h under 1.5 Sun UV light illumination. The 150–160 µm of epoxy layer was coated over the mPSCs and dried under vacuum overnight before the UV radiation exposure. mPSCs with epoxy showed a better stability under irradiation and humidity [17]. To improve PCE of these inkjet infiltrated mPSCs Hashmi et al. [18] suggested humidity assisted thermal exposure (HTE) as a post treatment The device kept for 200 h under HTE and shown significant enhancement in the average PCE from 9 to 13.1%, champion device shown 14.3% efficiency with high reproducibility [18].

4 Recommendation and concluding remarks

Among the PSCs architectures, mPSCs are the most promising candidate for the scalable fabrication since all the layers in mPSCs can be deposited using printable techniques. However, the PCE of the mPSCs is lower than that of conventional HTM-based PSCs. Also, the stability under continuous illumination and outdoor condition is also very crucial

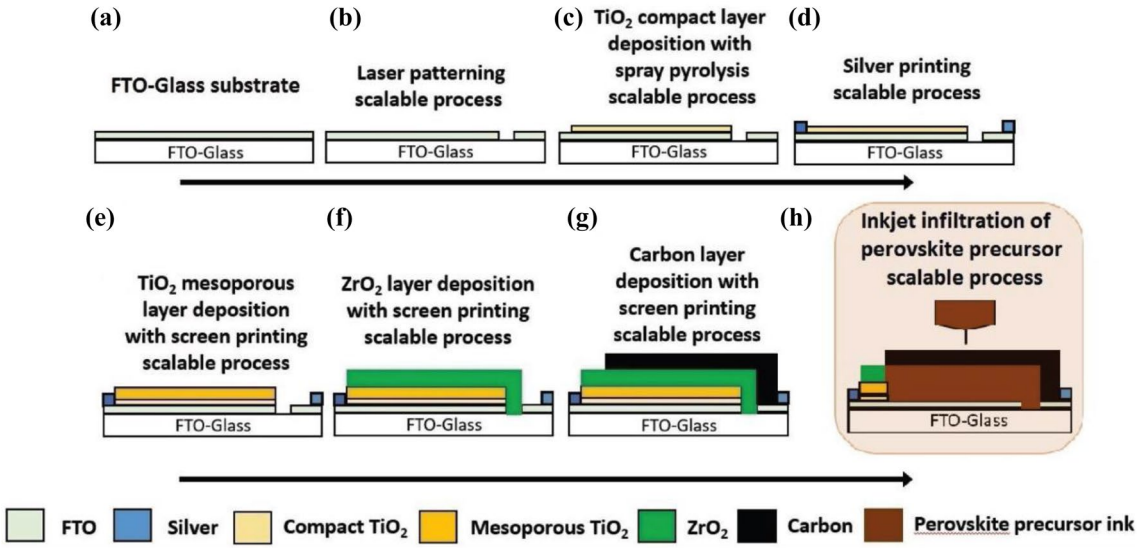

Fig. 5 Illustration of Fully printable scalable process for mPSCs fabrication. **a**, **b** FTO in glass substrate and its patterning through laser. **c** c-TiO_2 printing. **d**–**g** Screen printing of silver anode and cathode, mesoporous TiO_2, ZrO_2 and carbon electrodes. **h** Inkjet infiltration of perovskite precursor solution of fixed volume (Reprinted with permission from [16], copyright (2017) Wiley Online Library)

for commercialization. Therefore, improving the PCE and stability of the mPSCs is the priority of this time.

The fill factor and PCE of the mPSC is low due to the inadequate contact, low conductivity and low energy level matching between perovskite and carbon electrode [41]. The PCE of the large area mPSC modules can be enhanced by developing fullerene and graphene derivatives with improved conductivity and better energy levels alignment between perovskite and carbon electrode. The carbon counter electrode with smaller resistance can be prepared by modifying the combination of the conducting graphite and the catalyzing carbon black powders. The liquid metal (LM) as an interface modifier material can be combined with carbon paste to build a carbon electrode with enhanced conductivity. LMs can significantly increase the conductivity of the carbon electrode and optimize the contact property between carbon and perovskite [40]. Furthermore, series resistance can also be kept minimum by using FTO substrates with higher conductivities and without sacrificing optical transmittance. The active area of the module must be enlarged, while at the same time, the mismatch loss and internal resistance should be reduced by careful optimization of the module design.

In mPSCs, annealing of the carbon films is performed at 400°C, however this value of temperature has a negative impact on quality of carbon film [42]. Recent studies revealed the fast and atmospheric sintering process for perovskites films using intense pulsed light (IPL) technique [43]. By using this technique, it could be a future development to avoid the notable damage to the carbon films and better results can be achieved for quick and large area mPSCs fabrication. Application of ultraviolet light filter coating can be an optimistic perspective for large area mPSC. In similar fashion, some optimized & cost-effective encapsulation techniques could revolutionize the degradation problems in mPSCs. To enhance the long-term stability of mPSC hydrophobic additives must be explored. To avoid the degradation issue in mPSCs caused by the ultraviolet radiations, the use of multifunctional photopolymers is a promising solution [44]. The fluoropolymeric layer should be deposited on the front side of the device to block the UV light.

The 2D Ruddlesden–Popper perovskites attracted increasing research attention in recent years. The general formula of the 2D perovskite is $[(RNH_3)A_{n-1}B_nX_{3n+1}]$ where R is an aromatic group or long-chain alkyl have shown great stability as compared to 3D perovskites [45].. The capabilities of the other additives in $MAPbI_3$ such as carbon quantum dots (CQDs) [33], 4-(aminomethyl) benzoic acid hydroiodide (AB) [34], molten-salt [35], must be explored through inkjet printer.. Furthermore, perovskite precursor such as formamidinium lead triiodide ($Cs_{0.1}FA_{0.9}PbI_3$) [46] and methyl ammonium lead bromide ($MAPbBr_3$) [47] which have produced good results in small scale must be tested for larger scale printing with inkjet perovskite infiltration. For enabling other mesoporous layer inkjet printing, new inkjet printing compatible precursor inks must prepare.

Acknowledgement Open Access funding provided by the Qatar National Library. This publication was made possible by Qatar University Internal Grant Nos. QUCG-CAM-2018/19-1 and NPRP11S-1210-170080 from Qatar National Research Fund (a member of Qatar Foundation). The findings achieved herein are solely the responsibility of the authors.

Compliance with ethical standards

Conflict of interest The authors declare that there is no conflict of interest.

References

1. A. Kay, M. Grätzel, Low cost photovoltaic modules based on dye sensitized nanocrystalline titanium dioxide and carbon powder. Sol. Energy Mater. Sol. Cells **44**, 99–117 (1996)
2. Z. Ku, Y. Rong, M. Xu, T. Liu, H. Han, Full printable processed mesoscopic $CH_3NH_3PbI_3/TiO_2$ heterojunction solar cells with carbon counter electrode. Sci. Rep. **3**, 3132 (2013)
3. M. Xu, Y. Rong, Z. Ku, A. Mei, T. Liu, L. Zhang, X. Li, H. Han, Highly ordered mesoporous carbon for mesoscopic $CH_3NH_3PbI_3/TiO_2$ heterojunction solar cell. J. Mater. Chem. A **2**, 8607–8611 (2014)
4. Y. Rong, Z. Ku, A. Mei, T. Liu, M. Xu, S. Ko, X. Li, H. Han, Hole-conductor-free mesoscopic $TiO_2/CH_3NH_3PbI_3$ heterojunction solar cells based on anatase nanosheets and carbon counter electrodes. J. Phys. Chem. Lett. **5**, 2160–2164 (2014)
5. L. Zhang, T. Liu, L. Liu, M. Hu, Y. Yang, A. Mei, H. Han, The effect of carbon counter electrodes on fully printable mesoscopic perovskite solar cells. J. Mater. Chem. A **3**, 9165–9170 (2015)
6. A. Mei, X. Li, L. Liu, Z. Ku, T. Liu, Y. Rong, M. Xu, M. Hu, J. Chen, Y. Yang, M. Grätzel, H. Han, A hole-conductor–free, fully printable mesoscopic perovskite solar cell with high stability. Science (New York, N.Y.) **345**, 295 (2014)
7. L. Liu, A. Mei, T. Liu, P. Jiang, Y. Sheng, L. Zhang, H. Han, Fully printable mesoscopic perovskite solar cells with organic silane self-assembled monolayer. J. Am. Chem. Soc. **137**, 1790–1793 (2015)
8. Y. Yang, K. Ri, A. Mei, L. Liu, M. Hu, T. Liu, X. Li, H. Han, The size effect of TiO_2 nanoparticles on a printable mesoscopic perovskite solar cell. J. Mater. Chem. A **3**, 9103–9107 (2015)
9. T. Liu, L. Liu, M. Hu, Y. Yang, L. Zhang, A. Mei, H. Han, Critical parameters in TiO_2/ZrO_2/Carbon-based mesoscopic perovskite solar cell. J. Power Sources **293**, 533–538 (2015)
10. X. Li, M. Tschumi, H. Han, S.S. Babkair, R.A. Alzubaydi, A.A. Ansari, S.S. Habib, M.K. Nazeeruddin, S.M. Zakeeruddin, M. Grätzel, Outdoor performance and stability under elevated temperatures and long-term light soaking of triple-layer mesoporous perovskite photovoltaics. Energy Technol. **3**, 551–555 (2015)
11. J. Chen, Y. Rong, A. Mei, Y. Xiong, T. Liu, Y. Sheng, P. Jiang, L. Hong, Y. Guan, X. Zhu, X. Hou, M. Duan, J. Zhao, X. Li, H. Han, Hole-conductor-free fully printable mesoscopic solar cell with mixed-anion perovskite $CH_3NH_3PbI_{(3-x)}(BF_4)_x$. Adv. Energy Mater. **6**, 1502009 (2016)
12. D. Bi, W. Tress, M.I. Dar, P. Gao, J. Luo, C. Renevier, K. Schenk, A. Abate, F. Giordano, J.P. Correa Baena, J.D. Decoppet, S.M. Zakeeruddin, M.K. Nazeeruddin, M. Gratzel, A. Hagfeldt, Efficient luminescent solar cells based on tailored mixed-cation perovskites. Sci. Adv. **2**, e1501170 (2016)
13. Y. Sheng, Y. Hu, A. Mei, P. Jiang, X. Hou, M. Duan, L. Hong, Y. Guan, Y. Rong, Y. Xiong, H. Han, Enhanced electronic properties in $CH_3NH_3PbI_3$ via LiCl mixing for hole-conductor-free printable perovskite solar cells. J. Mater. Chem. A **4**, 16731–16736 (2016)
14. A.K. Baranwal, S. Kanaya, T.A. Peiris, G. Mizuta, T. Nishina, H. Kanda, T. Miyasaka, H. Segawa, S. Ito, 100 °C Thermal stability of printable perovskite solar cells using porous carbon counter electrodes. ChemSusChem **9**, 2604–2608 (2016)
15. X. Hou, Y. Hu, H. Liu, A. Mei, X. Li, M. Duan, G. Zhang, Y. Rong, H. Han, Effect of guanidinium on mesoscopic perovskite solar cells. J. Mater. Chem. A **5**, 73–78 (2017)
16. S.G. Hashmi, D. Martineau, X. Li, M. Ozkan, A. Tiihonen, M.I. Dar, T. Sarikka, S.M. Zakeeruddin, J. Paltakari, P.D. Lund, M. Grätzel, Air processed inkjet infiltrated carbon based printed perovskite solar cells with high stability and reproducibility. Adv. Mater. Technol. **2**(1), 1600183 (2017)
17. S.G. Hashmi, A. Tiihonen, D. Martineau, M. Ozkan, P. Vivo, K. Kaunisto, V. Ulla, S.M. Zakeeruddin, M. Grätzel, Long term stability of air processed inkjet infiltrated carbon-based printed perovskite solar cells under intense ultra-violet light soaking. J. Mater. Chem. A **5**, 4797–4802 (2017)
18. S.G. Hashmi, D. Martineau, M.I. Dar, T.T.T. Myllymäki, T. Sarikka, V. Ulla, S.M. Zakeeruddin, M. Grätzel, High performance carbon-based printed perovskite solar cells with humidity assisted thermal treatment. J. Mater. Chem. A **5**, 12060–12067 (2017)
19. Y. Hu, S. Si, A. Mei, Y. Rong, H. Liu, X. Li, H. Han, Stable large-area (10×10 cm^2) printable mesoscopic perovskite module exceeding 10% efficiency. Solar RRL **1**, 1600019 (2017)
20. J.A. Christians, F. Zhang, R.C. Bramante, M.O. Reese, T.H. Schloemer, A. Sellinger, M.F.A.M. van Hest, K. Zhu, J.J. Berry, J.M. Luther, Stability at scale: challenges of module interconnects for perovskite photovoltaics. ACS Energy Lett. **3**, 2502–2503 (2018)
21. A. Priyadarshi, L.J. Haur, P. Murray, D. Fu, S. Kulkarni, G. Xing, T.C. Sum, N. Mathews, S.G. Mhaisalkar, A large area (70 cm^2) monolithic perovskite solar module with a high efficiency and stability. Energy Environ. Sci. **9**, 3687–3692 (2016)
22. N. Alleborn, H. Raszillier, Spreading and sorption of droplets on layered porous substrates. J. Colloid Interface Sci. **280**, 449–464 (2004)
23. D.R. Heine, G.S. Grest, E.B. Webb 3rd, Surface wetting of liquid nanodroplets: droplet-size effects. Phys. Rev. Lett. **95**, 107801 (2005)
24. R. Holtzman, E. Segre, Wettability stabilizes fluid invasion into porous media via nonlocal, cooperative pore filling. Phys. Rev. Lett. **115**, 164501 (2015)
25. G. Grancini, C. Roldán-Carmona, I. Zimmermann, E. Mosconi, X. Lee, D. Martineau, S. Narbey, F. Oswald, F. De Angelis, M. Graetzel, M.K. Nazeeruddin, One-year stable perovskite solar cells by 2D/3D interface engineering. Nat. Commun. **8**, 15684 (2017)
26. A.D. Jodlowski, C. Roldán-Carmona, G. Grancini, M. Salado, M. Ralaiarisoa, S. Ahmad, N. Koch, L. Camacho, G. de Miguel, M.K. Nazeeruddin, Large guanidinium cation mixed with methylammonium in lead iodide perovskites for 19% efficient solar cells. Nat. Energy **2**, 972–979 (2017)
27. M. Saliba, T. Matsui, J.Y. Seo, K. Domanski, J.P. Correa-Baena, M.K. Nazeeruddin, S.M. Zakeeruddin, W. Tress, A. Abate, A. Hagfeldt, M. Gratzel, Cesium-containing triple cation perovskite solar cells: improved stability, reproducibility and high efficiency. Energy Environ. Sci. **9**, 1989–1997 (2016)
28. A.J. Huckaba, Y. Lee, R. Xia, S. Paek, V.C. Bassetto, E. Oveisi, A. Lesch, S. Kinge, P.J. Dyson, H. Girault, M.K. Nazeeruddin, Inkjet-printed mesoporous TiO_2 and perovskite layers for high efficiency perovskite solar cells. Energy Technol. **7**, 317–324 (2019)

29. A. Bashir, S. Shukla, J.H. Lew, S. Shukla, A. Bruno, D. Gupta, T. Baikie, R. Patidar, Z. Akhter, A. Priyadarshi, N. Mathews, S.G. Mhaisalkar, Spinel Co_3O_4 nanomaterials for efficient and stable large area carbon-based printed perovskite solar cells. Nanoscale **10**, 2341–2350 (2018)
30. N. Cheng, P. Liu, S. Bai, Z. Yu, W. Liu, S.-S. Guo, X.-Z. Zhao, Application of mesoporous SiO_2 layer as an insulating layer in high performance hole transport material free $CH_3NH_3PbI_3$ perovskite solar cells. J. Power Sources **321**, 71–75 (2016)
31. J. Zhao, Y. Zhang, X. Zhao, J. Zhang, H. Wang, Z. Zhu, Q. Liu, Band alignment strategy for printable triple mesoscopic perovskite solar cells with enhanced photovoltage. ACS Appl. Energy Mater. **2**(3), 2034–2042 (2019). https://doi.org/10.1021/acsaem.8b02104
32. Y. Guan, A. Mei, Y. Rong, M. Duan, X. Hou, Y. Hu, H. Han, Fullerene derivative as an additive for highly efficient printable mesoscopic perovskite solar cells. Org. Electron. **62**, 653–659 (2018)
33. H. Zou, D. Guo, B. He, J. Yu, K. Fan, Enhanced photocurrent density of HTM-free perovskite solar cells by carbon quantum dots. Appl. Surf. Sci. **430**, 625–631 (2018)
34. Y. Hu, Z. Zhang, A. Mei, Y. Jiang, X. Hou, Q. Wang, K. Du, Y. Rong, Y. Zhou, G. Xu, H. Han, Improved performance of printable perovskite solar cells with bifunctional conjugated organic molecule. Adv. Mater. **30**(11), 1705786 (2018)
35. L. Wagner, S. Chacko, G. Mathiazhagan, S. Mastroianni, A. Hinsch, High photovoltage of 1 V on a steady-state certified hole transport layer-free perovskite solar cell by a molten-salt approach. ACS Energy Lett. **3**, 1122–1127 (2018)
36. Y. Sheng, Y. Hu, A. Mei, P. Jiang, X. Hou, M. Duan, L. Hong, Y. Guan, Y. Rong, Y. Xiong, Enhanced electronic properties in $CH_3NH_3PbI_3$ via LiCl mixing for hole-conductor-free printable perovskite solar cells. J. Mater. Chem. A **4**, 16731–16736 (2016)
37. P. Liu, Y. Gong, Y. Xiao, M. Su, S. Kong, F. Qi, H. Zhang, S. Wang, X. Sun, C. Wang, X.Z. Zhao, Highly efficient and stable air-processed hole-transport-material free carbon based perovskite solar cells with caesium incorporation. Chem. Commun. (Camb.) **55**, 218–221 (2018)
38. B. Zong, W. Fu, Z.A. Guo, S. Wang, L. Huang, B. Zhang, H. Bala, J. Cao, X. Wang, G. Sun, Z. Zhang, Highly stable hole-conductor-free perovskite solar cells based upon ammonium chloride and a carbon electrode. J. Colloid Interface Sci. **540**, 315–321 (2019)
39. X. Hou, M. Xu, C. Tong, W. Ji, Z. Fu, Z. Wan, F. Hao, Y. Ming, S. Liu, Y. Hu, H. Han, Y. Rong, Y. Yao, High performance printable perovskite solar cells based on Cs0.1FA0.9PbI3 in mesoporous scaffolds. J. Power Sources **415**, 105–111 (2019)
40. Y. Zhang, J. Zhao, J. Zhang, X. Jiang, Z. Zhu, Q. Liu, Interface engineering based on liquid metal for compact-layer-free, fully printable mesoscopic perovskite solar cells. ACS Appl. Mater. Interfaces **10**, 15616–15623 (2018)
41. H.Z.Y. Wang, Y. Mei, H. Liu, S. Wang, X. Li, A carbon nanotube bridging method for hole transport layer-free paintable carbon-based perovskite solar cells. ACS Appl. Mater. Interfaces **11**(1), 916–923 (2018)
42. A. Mishra, Z. Ahmad, I. Zimmermann, D. Martineau, R.A. Shakoor, F. Touati, K. Riaz, S.A. Al-Muhtaseb, M.K. Nazeeruddin, Effect of annealing temperature on the performance of printable carbon electrodes for perovskite solar cells. Org. Electron. **65**, 375–380 (2019)
43. B.W.L.K. Ankireddy, T. Druffel, Atmospheric PROCESSING of perovskite solar cells using intense pulsed light sintering. J. Electron. Mater. **47**(2), 1285–1292 (2017)
44. G.G.F. Bella, J.P.C. Baena, G. Saracco, M. Grätzel, A. Hagfeldt, S. Turri, C. Gerbaldi, Improving efficiency and stability of perovskite solar cells with photocurable fluoropolymers. Science **354**(6309), 203–206 (2016)
45. S. Yu, Y. Yan, Y. Chen, P. Chábera, K. Zheng, Z. Liang, Enabling room-temperature processed highly efficient and stable 2D Ruddlesden-Popper perovskite solar cells with eliminated hysteresis by synergistic exploitation of additives and solvents. J. Mater. Chem. A **7**(5), 2015–2021 (2019)
46. X. Hou, M. Xu, C. Tong, W. Ji, Z. Fu, Z. Wan, F. Hao, Y. Ming, S. Liu, Y. Hu, High performance printable perovskite solar cells based on Cs0.1FA0.9PbI3 in mesoporous scaffolds. J. Power Sources **415**, 105–111 (2019)
47. Y. Liang, Y. Wang, C. Mu, S. Wang, X. Wang, D. Xu, L. Sun, Achieving high open-circuit voltages up to 1.57 V in hole-transport-material-free MAPbBr3 solar cells with carbon electrodes. Adv. Energy Mater. **8**, 1701159 (2018)